Current Optics and Photonics
Vol. 5, No. 4, August 2021, pp. 351–361

ISSN: 2508-7266(Print) / ISSN: 2508-7274(Online)
DOI: https://doi.org/10.3807/COPP.2021.5.4.351

Enhancement of Speckle Contrast *in vivo* by Combining Linearly Polarized Laser Light and an Analyzer

Muhammad Mohsin Qureshi[1], Khuong Duy Mac[1], Andrew Hyunjin Kim[2], Young Ro Kim[3,4], and Euiheon Chung[1,5]*

[1]*Department of Biomedical Science and Engineering, Gwangju Institute of Science and Technology, Gwangju 61005, Korea*
[2]*Department of Mechanical Engineering, The State University of New York Korea, Incheon 21985, Korea*
[3]*Athinoula A. Martinos Center for Biomedical Imaging, Massachusetts General Hospital, Charlestown, Massachusetts 02129, USA*
[4]*Department of Radiology, Harvard Medical School, Boston, Massachusetts 02115, USA*
[5]*AI Graduate School, Gwangju Institute of Science and Technology, Gwangju 61005, Korea*

(Received March 5, 2021 : revised April 16, 2021 : accepted April 21, 2021)

Speckle imaging is capable of dynamic data acquisition at high spatiotemporal resolution, and has played a vital role in the functional study of biological specimens. The presence of various optical scatterers within the tissue causes alteration of speckle contrast. Thus structures like blood vessels can be delineated and quantified. Although laser speckle imaging is frequently used, an optimization process to ensure the maximum speckle contrast has not been available. In this respect, we here report an experimental procedure to optimize speckle contrast via applying different combinations of varying polarization of the illuminating laser light and multiple analyzer angles. Specifically, samples were illuminated by the *p*-polarization, 45°-polarization, and *s*-polarization of the incident laser, and speckle images were recorded without and with the analyzer rotated from 0° to 180° ($\Delta = 30°$). Following the baseline imaging of a solid diffuser and a fixed brain sample, laser speckle contrast imaging (LSCI) was successfully performed to visualize in vivo mouse-brain blood flow. For oblique laser illumination, the maximum contrast achieved with *p*-polarized and *s*-polarized light was perpendicular to the analyzer's axis. This study demonstrates the optimization process for maximizing the speckle contrast, which can improve blood-flow estimation in vivo.

Keywords : Laser speckle imaging, Polarization, Speckle contrast
OCIS codes : (000.1430) Biology and medicine; (030.6140) Speckle; (110.6150) Speckle imaging; (170.0180) Microscopy

I. INTRODUCTION

Owing to wide range of applicability, the use of electromagnetic waves in biomedicine has been of high importance, effectively providing therapeutic and diagnostic means [1]. Moreover, significant recent advances in non-invasive optical imaging methods and analysis techniques have rendered distinctly powerful tools to investigate biological tissues in great detail, including functional characteristics in vivo [2, 3]. In particular, the characterization of light-tissue interactions (*i.e*. scattering and absorption coefficients) offers a unique option to understand biological tissue with excellent spatial and temporal resolutions [4–6]. The demand for such optical properties, obtained utilizing dynamic scattering, has significantly increased in recent years, for the documentation of tissue structures and their vascular features, such as the dynamic function of microfluidic channels [7–10].

*Corresponding author: ogong50@gist.ac.kr, ORCID 0000-0002-3326-6927
Color versions of one or more of the figures in this paper are available online.

For this purpose, several dynamic scattering techniques have been adopted for in vivo optical imaging, a highly utilized one being the speckle-based method. Advantages of speckle-based approaches include the capability of label-free, wide-field imaging with high spatial or temporal resolution, while requiring relatively simple instrumentation. In this regard, many speckle imaging techniques such as laser speckle contrast imaging (LSCI) [11, 12]; multi-exposure speckle imaging (MESI) [13], and the dynamic light scattering imaging model [14] have been proposed and used extensively in multiple areas of biomedical studies [15–17].

In such techniques, a time-varying speckle pattern is produced at each pixel of the image, providing dynamic information about the optical scatterers in the sample [18]. Time series of such speckle images with fluctuations of spatiotemporal intensity may be used to reveal dynamic movements, such as the flow of biological fluid [19]. The amount of speckle blurring can be quantified by the speckle contrast, ranging from 0 to 1. With laser speckle contrast a two-dimensional (2D) blood-flow map was obtained [11], and because of the 2D blood-flow map, laser speckle imaging has been adopted in clinical practice. LSCI is used extensively in ophthalmology to diagnose diseases such as retinopathy [20], glaucoma [21], and macular degeneration [22]. Furthermore, LSCI is also used for diagnostics of skin diseases [23–25].

To achieve a high-resolution blood-flow map, the laser contrast value should be high enough. To detect and quantify the blood flow accurately, LSCI requires optimization of speckle contrast. Several laser-speckle-imaging setups, including LSCI, MESI, and our previous studies [13, 26–30], have employed an analyzer (a linear polarizer) positioned before the camera to enhance the contrast value. However, the optimal setting conditions for the analyzer angle and laser polarization have not been demonstrated and discussed. In this regard, the current paper presents an experimental optimization based on three types of linear polarization of the illuminated laser, at different analyzer angles in the detection arm.

In laser speckle imaging, researchers have always tried to improve the speckle contrast, to observe the fine details of the sample and accurately quantify the blood flow [11, 13, 14, 31]. Therefore, it is important to observe the effect of the polarization of illuminating light experimentally. In this study, we illuminate the in vivo mouse brain before the detector analyzer is introduced. Three different types of incident laser polarization, which are *p*-polarization (*p*-pol), 45°-polarization (45°-pol), and *s*-polarization (*s*-pol), are used to illuminate the sample. We obtain speckle images without an analyzer and at different analyzer angles, for each type of polarized illumination. We also perform temporal LSCI (tLSCI) and spatial LSCI (sLSCI) on raw speckle images of the *in vivo* mouse brain, to observe the change in speckle contrast in the 2D blood-flow map. To the best of our knowledge, this study is the first in the literature to demonstrate the influence of three different linear polarizations of illumination and analyzer angles on in vivo mouse-brain data.

II. METHODS

2.1. Theory

The speckle contrast (K) is defined as

$$K = \frac{\sigma}{\langle I \rangle}, \tag{1}$$

where σ and $\langle I \rangle$ represent the standard deviation and mean intensity of the image respectively. The value of K is between 0 and 1. Ideally, if the scatterers are static, then the value of K is 1. As the scatterers move faster, K decreases, resulting in the smearing of the speckle. With the concept of speckle blurring, LSCI provides a 2D map of relative blood-flow velocity.

The tLSCI technique determines the K value for every frame pixel over a series of images, which results in higher spatial resolution; however, temporal resolution is sacrificed in the process. For tLSCI, K is defined in [20] as

$$K_{i,j} = \frac{\sigma_t}{\langle I \rangle} = \frac{\sqrt{\left[\left\langle I_{i,j,t}^2 \right\rangle_n - \left\langle I_{i,j,t} \right\rangle_n^2\right]}}{\left\langle I_{i,j,t} \right\rangle_n}, \tag{2}$$

where (i, j) is the pixel location over the number of image sequences, and n represents the number of images. In this study we employed 20 speckle images. For the sLSCI, a sliding window of size 5 × 5 pixels was adopted for the speckle contrast map [32], which was computed as

$$K_{i,j} = \frac{\boldsymbol{\sigma}_s}{\langle I \rangle} = \frac{\sqrt{\frac{1}{(1+n)^2}\sum_{x=i-n/2}^{i+n/2}\sum_{y=j-n/2}^{j+n/2} I_{x,y}^2 - \left(\frac{1}{(1+n)^2}\sum_{x'=i-n/2}^{i+n/2}\sum_{y'=j-n/2}^{j+n/2} I_{x',y'}^2\right)}}{\frac{1}{(1+n)^2}\sum_{x=i-n/2}^{i+n/2}\sum_{y=j-n/2}^{j+n/2} I_{x,y}^2}. \tag{3}$$

Here polarization is defined by the electric field ($\vec{E}$) vector perpendicular to the propagation of the coherent light wave. In addition, the complex field is defined by the Jones vector [33]:

$$\vec{E} = \begin{bmatrix} E_x \\ E_y \end{bmatrix} = \begin{bmatrix} E_{0x} e^{i(kz-\omega t+\varphi_x)} \\ E_{0y} e^{i(kz-\omega t+\varphi_y)} \end{bmatrix}, \tag{4}$$

where k and ω represent the wave number and angular frequency respectively. For linearly polarized light, the difference between φ_x and φ_y is zero, *i.e.*, $\Delta\omega = \varphi_x - \varphi_y = 0$.

2.2. Optical Setup

The optical setup adopted in this study is illustrated in Fig. 1. A helium-neon (HeNe) laser (Research Electro-Optics Inc., Colorado, USA) with wavelength and output power of 632 nm and 17 mW, respectively, was employed for speckle imaging. The output beam was expanded twice, by combining two convex lenses (focal lengths f_1 = 100 mm and f_2 = 50 mm). A neutral density filter NDC-50C-4

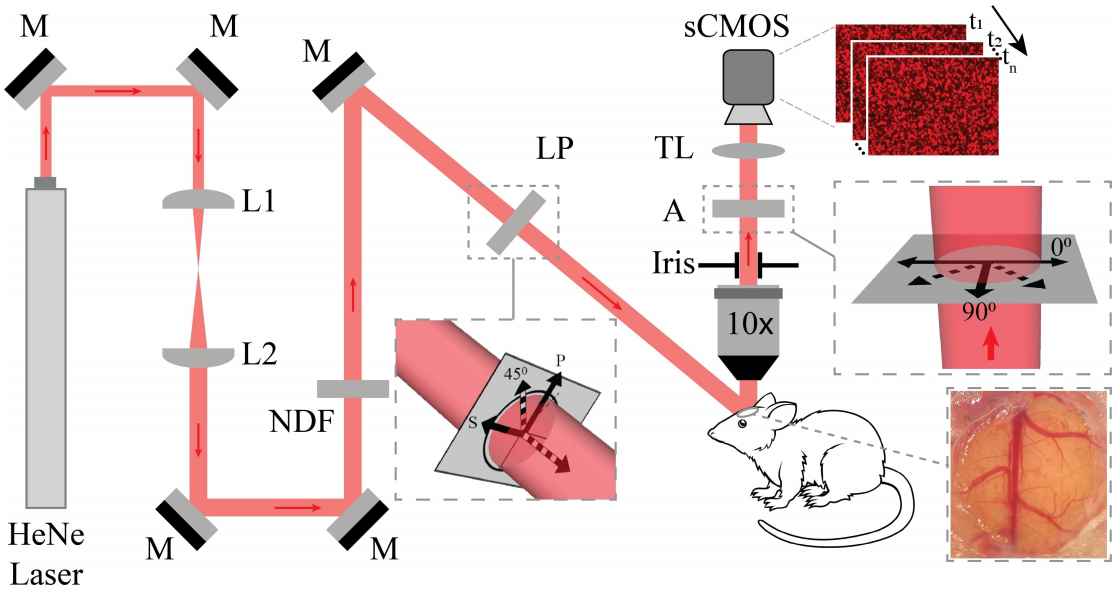

FIG. 1. Diagram of the optical setup. The optical setup consists of a He-Ne laser with a wavelength of 632.8 nm. The laser beam is steered to a pair of convex lenses of focal lengths f_1 = 100 mm and f_2 = 50 mm. A linear polarizer is adopted to set the polarization of illuminating laser light to *p*-pol, 45°-pol, and *s*-pol. Then the laser light is illuminated upon the sample. The light reflected from the sample is captured by an sCMOS camera after passing through a 10× objective lens, iris, analyzer, and tube lens. An analyzer is used perform rotations from 0° to 180°. M, mirrors; L1 and L2, convex lenses; LP, linear polarizer; NDF, neutral density filter; A, analyzer; TL, tube lens.

(Thorlabs, NJ, USA) was utilized to control the laser power before introducing the linear polarizer WP25M-VIS (Thorlabs, NJ, USA). The purpose of the neutral density filter was to keep constant the irradiance of laser light over the whole sample, for every polarization of illumination of light.

To collect the reflected light from the sample, a 10× objective lens, Olympus Plan Achromat Microscope Objective 10×, 0.25 NA, RMS10X (Thorlabs, NJ, USA) was used together with the iris to control the speckle size. The speckle size was approximately 3 × 3 pixels on the camera's sensor, which satisfies the Nyquist criteria. An analyzer WP25M-VIS (Thorlabs, NJ, USA) was positioned between the objective lens and tube lens (focal length 180 mm) to image the speckle on the sCMOS camera Neo 5.5 sCMOS (Andor Technology Ltd., Belfast, UK). The region of interest (ROI) was 1392 × 1040 pixels (900 × 670 μm^2), and the acquisition of data was performed with minimum exposure time and frame rate of 12.5 ms and 80 fps respectively.

Here we adopted three different linear polarizations of light (*p*-pol, 45°-pol, and *s*-pol) to illuminate the sample with the same laser power, adjusted by a neutral density filter. For each illuminating laser light, speckle images were obtained without an analyzer and with an analyzer angled at 0°, 30°, 60°, 90°, 120°, and 150°.

2.3. Sample Preparation

For the static diffuser experiment, a solid diffuser DG10-220 (Thorlabs, NJ, USA) was set on the sample holder MP100-RCH1 (Thorlabs, NJ, USA) and speckle images were obtained. We also adopted an ex vivo fixed brain sample in 4% paraformaldehyde (PFA) solution. First the fixed brain was rinsed with phosphate-buffered solution (1× PBS), and then a drop of the acrylic-glue-fixed brain was placed on the microscope slide. Next a cover slip was positioned on top of the fixed brain sample.

Furthermore, for the in vivo experiment we carried out all animal handling at the Gwangju Institute of Science and Technology, Korea, in accordance with Institutional Animal Care and Use Committee (IACUC) guidelines. The Laboratory Animal Resource Center, Gwangju Institute of Science and Technology, South Korea (Protocol Number: GIST-2020-084) approved the protocol and procedures. In the experiment we used 12–14-week-old C57BL/6 black mice. The mice were anesthetized with Zoletil/Xylazine mixture in a saline solution (60/10 mg/kg body weight). The body temperature of the mice was maintained at 37–37.5 °C. For craniotomy and further imaging, we followed the procedure described in the literature [34–36]. To fix the head of mouse to the heating system, we employed a special, customized ring-type in vivo heating system (Live Cell Instruments, Seoul, South Korea) [37].

2.4. Data Processing

To compute the mean values and standard deviations for each observation, we used ten images (n = 10). Furthermore, on the raw speckle images the tLSCI and sLSCI algorithms were implemented in MATLAB R2018. For

tLSCI, 20 images were used for the inverse contrast ($1/K$) map of the in vivo data. For the sLSCI, a 5 × 5 pixel window was employed to create the $1/K$ map. Moreover, to compare tLSCI to sLSCI we averaged 20 $1/K$ maps.

III. RESULTS

To observe the effect of light polarization and analyzer on the speckle contrast, we conducted a solid-diffuser experiment and used a fixed brain sample, followed by an in vivo experiment. For detailed analysis, we measured the mean intensity and speckle contrast of the images, and also performed sLSCI and tLSCI on the raw speckle images.

3.1. Characterization of Linearly Polarized Incident Light and Analyzer

We experimented with a solid diffuser to calibrate the baseline for our system and linear polarizer of the illumination laser, as illustrated in Fig. 2. A solid optical diffuser was positioned on the stage while the sample was irradiated with laser light at an oblique angle, as shown in Fig. 2(a). The speckle image was formed on the sCMOS sensor, with a speckle size of approximately 3 pixels, as presented in Fig. 2(b). The obtained histograms of the raw speckle images indicate that the speckles were fully developed. To elaborate the effect of the analyzer on speckle contrast, a graph with no analyzer (green area) and analyzer angle (red area) on the x axis and mean intensity on the y axis is shown in Fig. 2(c). The mean intensity value decreased as the analyzer was placed in the optical system. For all three types of linearly polarized light, the mean intensity varied with a sinusoidal trend. The maximum values for s-pol, 45°-pol, and p-pol were at analyzer angles of 90°, 120°, and 0° respectively.

Speckle contrast improved when the analyzer was in

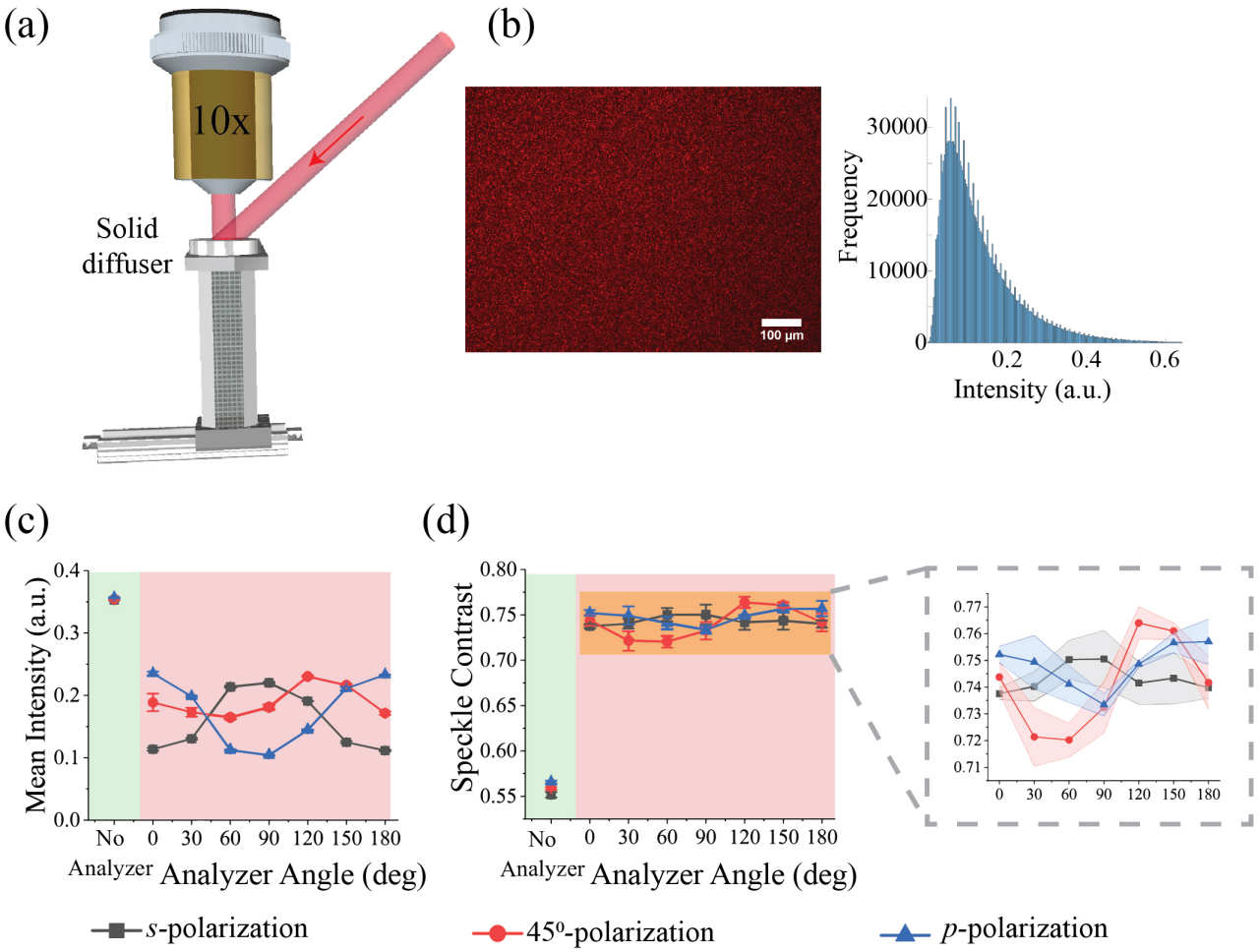

FIG. 2. Characterization of illuminating light and imaging system. (a) Solid-diffuser experimental setup. Polarized light illuminates the sample, and the reflected light forms speckles on the sCMOS, (b) Sample speckle image (900 × 670 μm^2) and histogram for the characterization of speckles, (c) mean intensity graph for the no analyzer condition (green), and at different analyzer angles (red), and (d) relationship between the analyzer angle and speckle contrast for the solid phantom. The inset presents detailed variations of speckle contrasts for s-, 45°-, and p-polarized incident laser light. The number of trials n for each observation was 10. The data points represent the mean intensity and standard deviation values.

place. The graph of speckle contrast versus the no analyzer condition and analyzer angle is shown in Fig. 2(d). The speckle contrast increased with the use of an analyzer. The maximum values of speckle contrast for *s*-pol, 45°-pol, and *p*-pol were 0.750 ± 0.01 at 0°, 0.760 ± 0.006 at 120°, and 0.750 ± 0.01 at 0° respectively. The change in speckle contrast across all analyzer angles was not significant.

3.2. Speckle-contrast Variation with the Fixed Brain Sample

The solid-diffuser experiment was a suitable experiment for the initial characterization of the illuminating light and analyzer angle. However, before carrying out the in vivo experiment, we conducted an ex vivo experiment in which we adopted a fixed mouse brain as the sample. The fixed brain is an optimal sample for imaging, because it has a morphology similar to that of an in vivo mouse brain. The sample was fixed on a microscope slide, as illustrated in Fig. 3(a). To check whether the speckles were fully developed, we prepared a speckle image histogram, as presented in Fig. 3(b).

The mean intensities of the images at different analyzer angles are presented in Fig. 3(c). Concerning the mean intensities for the no analyzer condition (green area), because the power of the input laser beam was controlled, all of the intensity values in the green region were nearly equal. For different analyzer angles (red region), the intensity-variation pattern was similar to that in the solid-diffuser experiment presented in Fig. 2(c). This indicates that the *p*-polarized light exhibited maximum mean intensity at 0°, whereas the *s*-polarized light exhibited a maximum value at 90°. Finally, the 45°-pol case exhibited a maximum value at 120°.

The speckle contrast varied with changes in both incident-light polarization and analyzer angle at the detector, as presented in Fig. 3(d). The speckle contrast for the no analyzer condition (green region) is lower than that for the analyzer condition (red region), for all three types of polarization. The speckle contrast for the *p*-pol, 45°-pol, and *s*-pol cases exhibited maximum values of 0.740 ± 0.003 at 90°, 0.740 ± 0.004 at 120°, and 0.750 ± 0.001 at 0° respectively.

3.3. Improvement of Speckle Contrast for *In Vivo* Mouse Brain

After the solid-diffuser and fixed brain samples, we observed the effect of various analyzer angles on speckle contrast for the in vivo mouse brain. Using Eq. (2), we performed tLSCI on 20 speckle images for each angle; the averaged images thus obtained are presented in Fig. 4. To improve visual clarity, we present the 1/*K* images. The

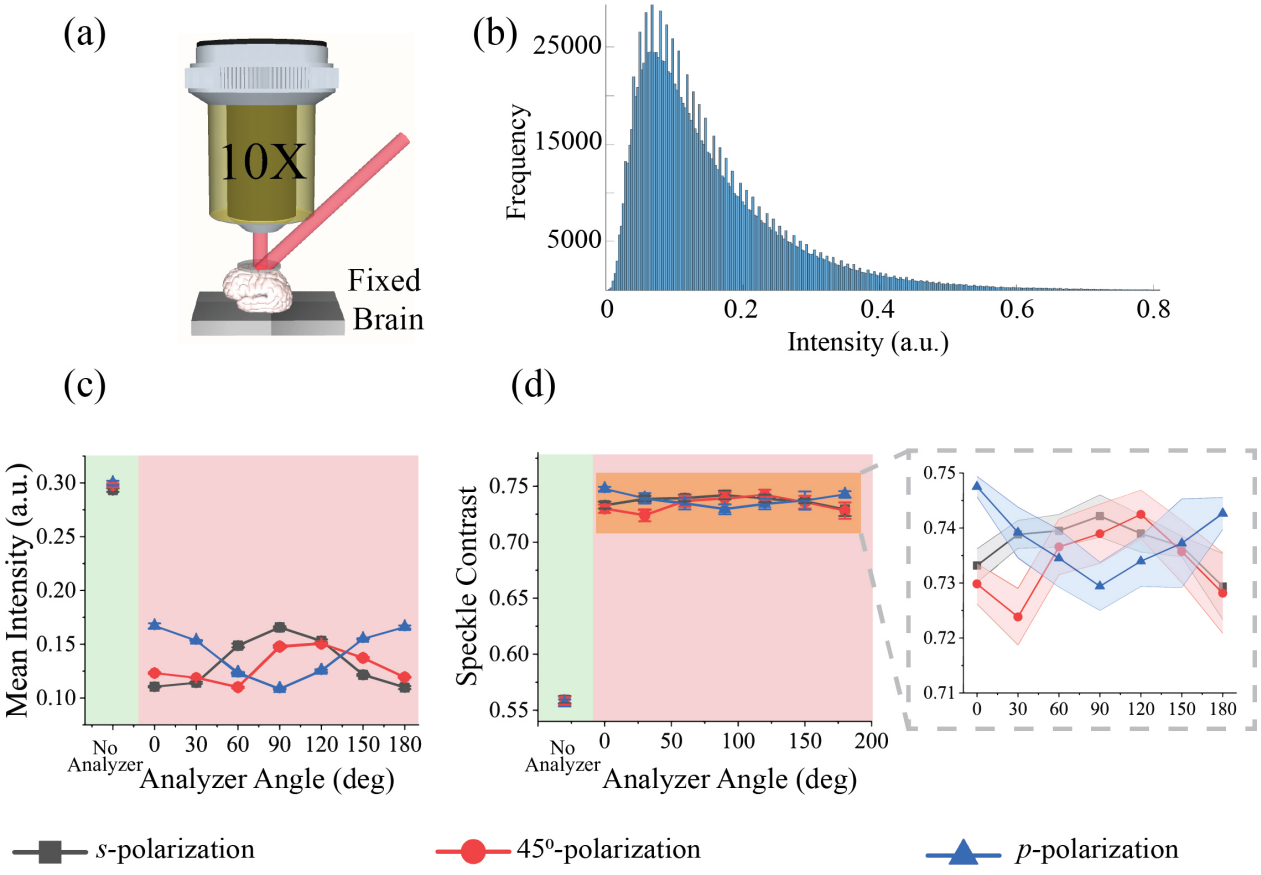

FIG. 3. Variations in mean intensity and speckle contrast for the fixed brain sample. (a) Setup for the ex vivo fixed brain sample for *p*-, 45°-, and *s*-polarized incident laser light, (b) mean intensity graph, and (c) speckle contrast graph, for the no analyzer condition (green) and at different analyzer angles (red).

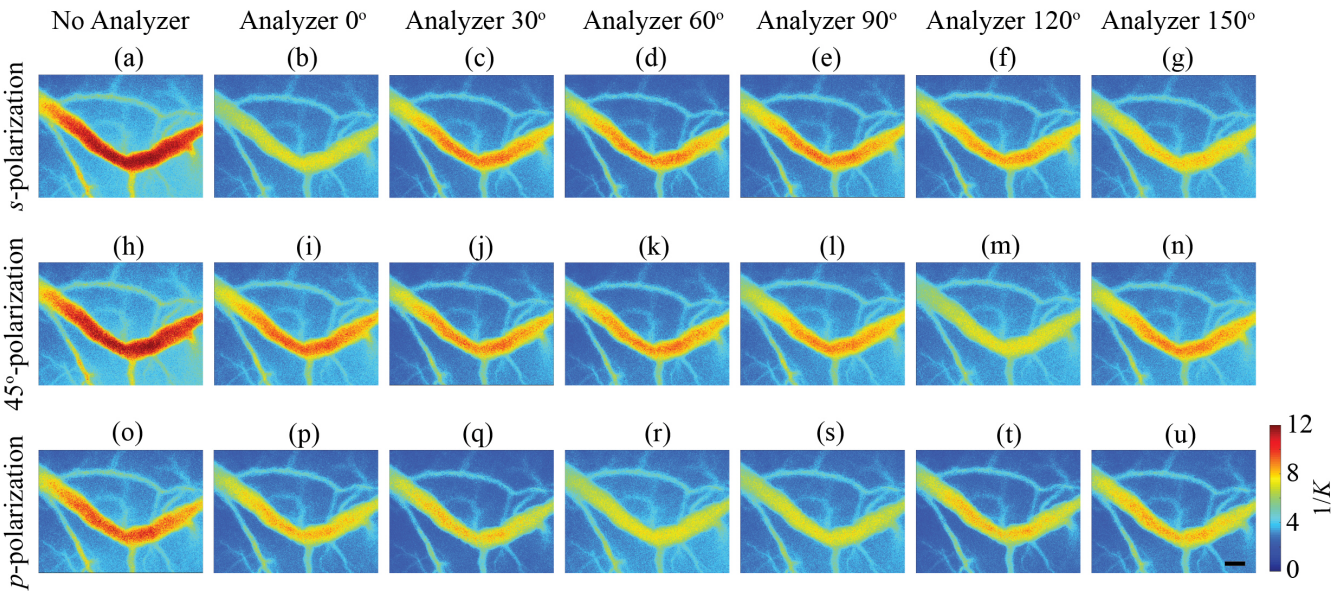

FIG. 4. In vivo mouse cortex tLSCI for the different polarizations of illuminating light. The value at each pixel make the blood vessels and brain tissue visible. 20 images were averaged for each tLSCI map. The no analyzer condition is presented in (a), (h), and (o) for *p*-pol, 45°-pol, and *s*-pol illuminating light respectively. For *p*-pol illumination, (b)–(g) present tLSCI maps for the analyzer at 0°, 30°, 60°, 90°, 120°, and 150°, while (i)–(n) and (p)–(u) provide the tLSCI maps for the 45°- and *s*-polarized laser light respectively (Image size: 0.9 mm × 0.7 mm).

tLSCI images for the no analyzer condition for the *s*-pol, 45°-pol, and *p*-pol cases are presented in Figs 4(a), 4(h), and 4(o) respectively. In all cases the $1/K$ value was higher with an analyzer than without. In other words, K improved by introducing an analyzer. For the *s*-pol case, the minimum $1/K$ was found at an analyzer angle of 90°, as in Fig. 4(b). The tLSCI map in Fig. 4(e) displays a relatively large $1/K$ value at 90°. However, at 90° the speckle contrast was better than that for the no analyzer condition. The minimum $1/K$ value was found for the 45°-pol illumination case (as shown in Fig. 4(m)) when the analyzer angle was set at 120°. Finally, for the *p*-pol case the minimum $1/K$ value was at 0°, as shown in Fig. 4(s). It is demonstrated that at any analyzer angle, the $1/K$ values for all three cases were better with the analyzer than under no analyzer conditions. We also obtained the average sLSCI from 20 images for, as presented in Fig. A1 of the Appendix.

A graph of mean intensity and mean speckle contrast versus analyzer angle for *s*-pol, 45°-pol, and *p*-pol for the in vivo mouse brain speckle images is presented in Fig. 5(a). Seven analyzer angles with stepwise 30° increments were selected to determine the mean intensity and speckle contrast. For the *s*-pol case, the speckle contrast maximum value of 0.700 ± 0.006 was found at an analyzer angle of 0°, its value varying sinusoidally, reaching a minimum value of 0.540 ± 0.016 at 90°. Although the variations in mean intensity also followed the same trend, these changes were negligible. For the 45°-pol illumination case, the maximum and minimum values of the speckle contrast were 0.690 ± 0.008 and 0.580 ± 0.014 at analyzer angles of 120° and 30°. For the *p*-pol case, the mean speckle contrast's maximum value of 0.710 ± 0.013 was found at 90°, whereas the minimum value of 0.600 ± 0.010 was at 180°, reversed in comparison to the case of *s*-pol illumination.

A comparison of the mean intensity with and without the analyzer is presented in Fig. 5(b). With the analyzer, the intensity decreased by approximately 50% for all polarizations. An inset is provided for all analyzer angles in Fig. 5(b), in which the resulting intensity exhibits a fluctuation trend similar to that found for the speckle contrast. However, no statistically significant difference was observed among all of the mean intensity values.

Similarly, a comparison of the speckle contrasts for the no analyzer condition and at different analyzer angles is presented in Fig. 5(c). For the *s*-pol case, the speckle contrast increased or remained at the same level when the analyzer was positioned in the optical system. For *p*-pol illumination, the speckle contrast decreased at analyzer angles of 60° and 90° and was less than when measured under the no analyzer condition. Furthermore, for the 45°-pol case, the speckle-contrast values are in general greater than those under the no analyzer condition, except for the analyzer angle of 30°.

To test whether the speckle-contrast trend shown in Fig. 5(c) persisted in another biological tissue, we performed speckle imaging of a nude mouse ear, and show a comparison in Fig. A2. From this comparison, we conclude that the trend in changing speckle contrast is similar for both mouse brain and nude mouse ear.

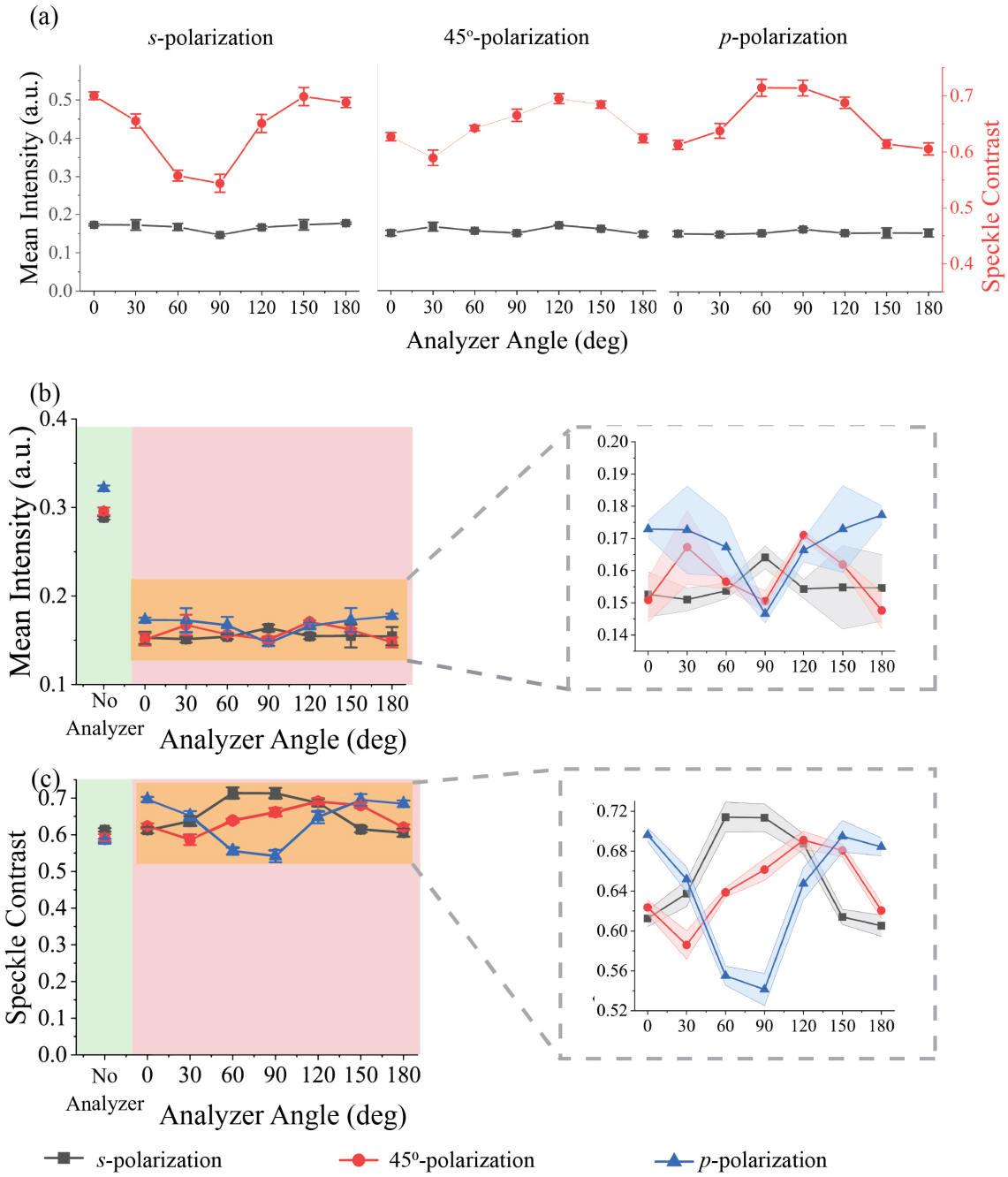

FIG. 5. Comparison of speckle contrast to mean intensit for different incident-light polarizations at known analyzer angles. (a) Graph showing the relationship between mean intensity, speckle contrast, and analyzer angle for *p*-, 45°-, and *s*-polarized light, (b) mean intensity for the analyzer angle and no analyzer conditions, and (c) speckle contrast versus analyzer angle, with the traces for the three polarization cases overlapping each other. This graph is provided to elucidate the speckle-contrast trend relative to the analyzer angle and no analyzer conditions. In (b) and (c), green represents the no analyzer zone, while red indicates the analyzer angle zone.

IV. DISCUSSION AND CONCLUSION

The speckle contrast (K) is defined as the ratio of the standard deviation to the mean intensity of an image. The value of the speckle contrast ranges from zero to one, and the maximum possible speckle contrast is required for the best imaging. In general, implementing an analyzer (a linear polarizer) before the sensor is an effective technique for improving the speckle contrast. To investigate the optimal imaging conditions, the current study presents comprehensive experimental results for speckle contrast and mean intensity, quantified for three types of linear polarization at different analyzer angles. Specifically, the illuminating light was polarized as *s*-pol, 45°-pol, and *p*-pol, at analyzer angles of 0°, 30°, 60°, 90°, 120°, 150°, and 180°.

From the results for a solid phantom, ex vivo sample

(fixed brain), and in vivo mouse brain, we conclude that it is always better to adopt an analyzer to improve the speckle contrast, which results in an approximately 35% increase in speckle contrast value for the solid-phantom and fixed brain samples. For in vivo imaging, the speckle contrast increased by approximately 15% with the analyzer. In contrast, when the analyzer was used the mean intensity decreased, because it passes only the light that is polarized in the direction of the analyzer angle. The mean intensity decreased by approximately 25% and 40% for the solid diffuser and fixed brain respectively, and for the in vivo sample it decreased by around 45%. Therefore, with a low-power laser a tradeoff between speckle contrast and intensity must be considered, for further optimization of the optical setup.

For the solid-diffuser and fixed brain samples, the change in speckle contrast over all analyzer angles was always less than 5%, for all three linear polarizations of the incident light. However, for the in vivo mouse brain the maximum speckle contrast for *s*-polarized laser light could be achieved at an analyzer angle of 90°, which was 15% greater than the minimum speckle contrast at 0°. For the *p*-polarized laser, the maximum value was obtained at 0°, and it was also 15% greater than the minimum speckle contrast at 90°, whereas the maximum speckle contrast for the 45°-polarized laser was obtained at 120°.

For the maximum contrast at the perpendicular setting of illumination polarization and analyzer angle, direct reflection (or a single scattering) from the medium's surface may not carry much information about the scattering medium. While this contributes to increased mean intensity, speckle contrast can be maximized with multiply scattered light (*i.e.* more chances for changing polarization direction) within the medium. Thus, when the analyzer is perpendicular to the illumination, the transmitted light carries more information about the dynamics of the medium, hence the higher speckle contrast. Furthermore, in the future, Monte Carlo simulation [38, 39] could be performed for linear, circular, and elliptical polarizations of illumination, for biological tissue. We also plan to test whether this result holds for other illumination angles.

In this study we considered only the linear polarization effect, which could be a limiting factor. For future research, investigation of circular or elliptical polarization effects on a biological sample is warranted, to optimize the speckle contrast further. Moreover, a single wavelength (a 632-nm HeNe laser) was used in this study, which could be an additional limiting factor. Owing to the significant dependence of the absorption and scattering coefficients on wavelength, a detailed study is required in the future. Furthermore, among the three types of polarized illumination for *s*-pol and *p*-pol light the maximum contrast was achieved at a perpendicular analyzer angle. However, for 45°-pol illumination the maximum contrast lay between analyzer angles of 120° and 150°. Therefore, in the future smaller angle steps would reveal more details.

In conclusion, this study provides experimental results for different linear light polarizations for in vivo speckle imaging at different analyzer angles. The analyzer angle should be perpendicular in the cases of *s*-pol and *p*-pol illumination.

APPENDIX

I. Spatial LSCI

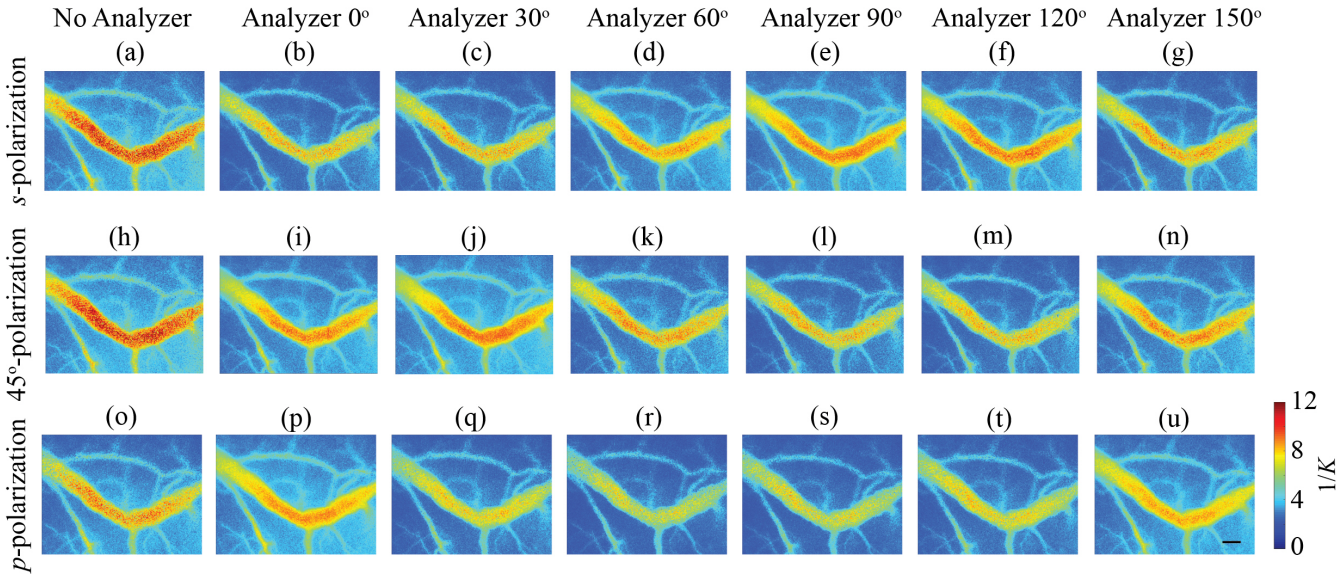

FIG. A1. In vivo mouse cortex averaged sLSCI for the different polarizations of illuminating light. The $\frac{1}{K}$ value for each pixel make the blood vessels and brain tissue visible. 20 images were averaged for each sLSCI map of $\frac{1}{K}$; the window size was 5 × 5 pixels. The no analyzer condition is shown in (a), (h), and (o) for *p*-pol, 45°-pol, and *s*-pol illumination respectively. For *p*-pol illumination, (b–g) show the sLSCI maps for analyzer angles of 0°, 30°, 60°, 90°, 120°, and 150°, while (i–n) give sLSCI maps for 45°-pol laser light, and (p–u) show the maps for *s*-pol light (Image size: 0.9 × 0.7 mm).

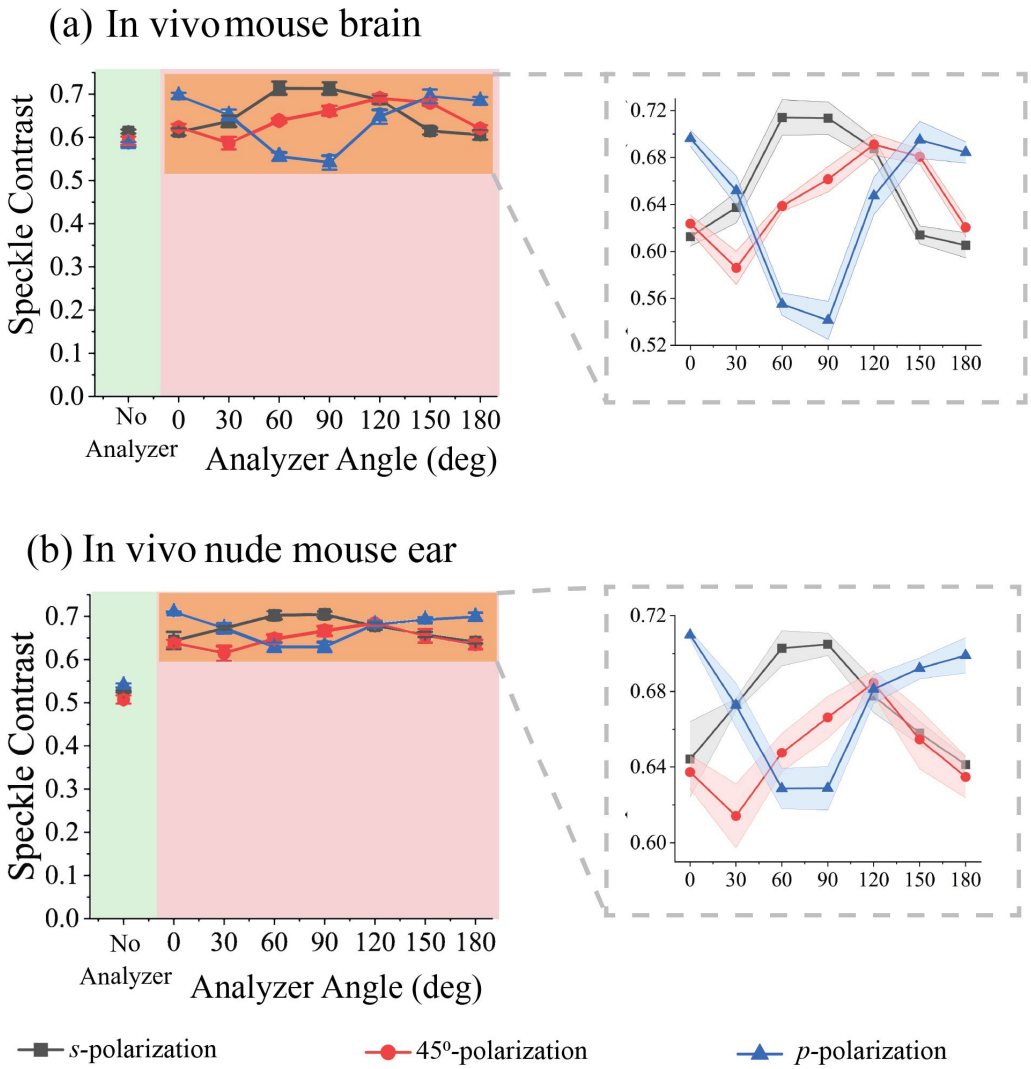

FIG. A2. Comparison of speckle contrast for in vivo mouse brain cortex and nude mouse ear, for different polarizations of illuminating laser light. For the no analyzer condition and different analyzer angles from 0° to 180°, the speckle contrast is calculated for (a) mouse brain and (b) nude mouse ear. From (a) and (b) we can observe that the trend in changing speckle contrast is similar for both biological samples.

ACKNOWLEDGMENT

This work was supported by the GIST Research Institute (GRI) GIST-CNUH research collaboration grant, funded by GIST in 2021 and the Joint Research Project of the Institutes of Science and Technology in 2021. This work was supported by the Institute of Information & Communications Technology Planning & Evaluation (IITP) grant, funded by the Korea government (MSIT) (No.2019-0-01842, Artificial Intelligence Graduate School Program (GIST)). This research was also supported by the National Research Foundation of Korea (NRF), funded by the Korean government (MEST) (NRF-2019R1A2C2086003), and the Brain Research Program through the NRF, funded by the Ministry of Science, ICT & Future Planning (NRF-2017M3C7A1044964), and finally by the Ministry of Science and ICT, the Ministry of Trade, Industry and Energy, the Ministry of Health & Welfare, Republic of Korea, and the Ministry of Food and Drug Safety (Project Number: 202011D13).

REFERENCES

1. R. K. Amineh, "Applications of electromagnetic waves: present and future," Electronics **9**, 808 (2020).
2. S. Costanzo and G. Lopez, "Phaseless microwave tomography assessment for breast imaging: preliminary results," Int. J. Antennas Propag. **2020**, 5780243 (2020).
3. W. Mier and D. Mier, "Advantages in functional imaging of the brain," Front. Hum. Neurosci. **9**, 249 (2015).
4. D. A. Boas, C. Pitris, and N. Ramanujam, *Handbook of Biomedical Optics* (CRC Press, FL, USA. 2011).

5. L. V. Wang and Hsin-I Wu, *Biomedical Optics: Principles and Imaging* (John Wiley & Sons, NJ, USA. 2012).
6. E. Chung and A. Vitkin, "Photon mayhem: new directions in diagnostic and therapeutic photomedicine," Biomed. Eng. Lett. **9**, 275-277 (2019).
7. M. Aswendt, J. Adamczak, and A. Tennstaedt, "A review of novel optical imaging strategies of the stroke pathology and stem cell therapy in stroke," Front. Cell. Neurosci. **8**, 226 (2014).
8. E. A. Rodriguez, G. N. Tran, L. A. Gross, J. L. Crisp, X. Shu, J. Y. Lin, and R. Y. Tsien, "A far-red fluorescent protein evolved from a cyanobacterial phycobiliprotein," Nat. Methods **13**, 763–769 (2016).
9. A. Arranz and J. Ripoll, "Advances in optical imaging for pharmacological studies," Front. Pharmacol. **6**, 187 (2015).
10. P. K. Poola, M. I. Afzal, Y. Yoo, K. H. Kim, and E. Chung, "Light sheet microscopy for histopathology applications," Biomed. Eng. Lett. **9**, 279–291 (2019).
11. A. K. Dunn, H. Bolay, M. A. Moskowitz, and D. A. Boas, "Dynamic imaging of cerebral blood flow using laser speckle," J. Cereb. Blood Flow Metab. **21**, 195–201 (2001).
12. D. A. Boas and A. K. Dunn, "Laser speckle contrast imaging in biomedical optics," J. Biomed. Opt. **15**, 011109 (2010).
13. A. B. Parthasarathy, W. J. Tom, A. Gopal, X. Zhang, and A. K. Dunn, "Robust flow measurement with multi-exposure speckle imaging," Opt. Express **16**, 1975-1989 (2008).
14. D. D. Postnov, J. Tang, S. E. Erdener, K. Kiliç, and D. A. Boas, "Dynamic light scattering imaging," Sci. Adv. **6**, eabc4628 (2020).
15. R. A. Leitgeb, L. Schmetterer, W. Drexler, A. F. Fercher, R. J. Zawadzki, and T. Bajraszewski, "Real-time assessment of retinal blood flow with ultrafast acquisition by color Doppler Fourier domain optical coherence tomography," Opt. Express **11**, 3116–3121 (2003).
16. H. Li, Q. Liu, H. Lu, Y. Li, H. F. Zhang, and S. Tong, "Directly measuring absolute flow speed by frequency-domain laser speckle imaging," Opt. Express **22**, 21079–21087 (2014).
17. A. Rege, K. Murari, A. Seifert, N. V. Thakor, and A. P. Pathak, "Multiexposure laser speckle contrast imaging of the angiogenic microenvironment," J. Biomed. Opt. **16**, 056006 (2011).
18. J. W. Goodman, *Speckle Phenomena in Optics: Theory and Applications* (Ben Roberts & Company, CO, USA. 2007).
19. J. D. Briers and S. Webster, "Laser speckle contrast analysis (LASCA): a nonscanning, full-field technique for monitoring capillary blood flow," J. Biomed. Opt. **1**, 174–179 (1996).
20. T. Sugiyama, M. Araie, C. E. Riva, L. Schmetterer, and S. Orgul, "Use of laser speckle flowgraphy in ocular blood flow research," Acta Ophthalmol. **88**, 723–729 (2010).
21. Y. Tamaki, M. Araie, K. Tomita, M. Nagahara, A. Tomidokoro, and H. Fujii, "Real-time measurement of human optic nerve head and choroid circulation, using the laser speckle phenomenon," Jpn. J. Ophthalmol. **41**, 49–54 (1997).
22. X. Wei, P. K. Balne, K. E. Meissner, V. A. Barathi, L. Schmetterer, and R. Agrawal, "Assessment of flow dynamics in retinal and choroidal microcirculation," Surv. Ophthalmol. **63**, 646–664 (2018).
23. A. D. Rossa, M. Cazzato, A. D'Ascanio, A. Tavoni, W. Bencivelli, P. Pepe, M. Mosca, C. Baldini, M. Rossi, and S. Bombardieri, "Alteration of microcirculation is a hallmark of very early systemic sclerosis patients: A laser speckle contrast analysis," Clin. Exp. Rheumatol. **31**, 109–114 (2013).
24. F. Gaillard-Bigot, M. Roustit, S. Blaise, M. Gabin, C. Cracowski, C. Seinturier, B. Imbert, P. Carpentier, and J. L. Cracowski, "Abnormal amplitude and kinetics of digital postocclusive reactive hyperemia in systemic sclerosis," Microvasc. Res. **94**, 90–95 (2014).
25. B. Ruaro, A. Sulli, E. Alessandri, C. Pizzorni, G. Ferrari, and M. Cutolo, "Laser speckle contrast analysis: a new method to evaluate peripheral blood perfusion in systemic sclerosis patients," Ann. Rheum. Dis. **73**, 1181–1185 (2014).
26. J. D. Briers, G. J. Richards, and X.-W. He, "Capillary blood flow monitoring using laser speckle contrast analysis (LASCA)," J. Biomed. Opt. **4**, 164–175 (1999).
27. J. D. Briers, "Laser speckle contrast imaging for measuring blood flow," Opt. Appl. **37**, 139–152 (2007).
28. T. Dragojević, D. Bronzi, H. M. Varma, C. P. Valdes, C. Castellvi, F. Villa, A. Tosi, C. Justicia, F. Zappa, and T. Durduran, "High-speed multi-exposure laser speckle contrast imaging with a single-photon counting camera," Biomed. Opt. Express **6**, 2865–2876 (2015).
29. L. M. Richards, E. L. Towle, D. J. Fox, and A. K. Dunn, "Intraoperative laser speckle contrast imaging with retrospective motion correction for quantitative assessment of cerebral blood flow," Neurophotonics **1**, 015006 (2014).
30. H.-J. Jeon, M. M. Qureshi, S. Y. Lee, J. D. Badadhe, H. Cho, and E. Chung, "Laser speckle decorrelation time-based platelet function testing in microfluidic system," Sci. Rep. **9**, 16514 (2019).
31. M. M. Qureshi, Y. Liu, K. D. Mac, M. Kim, A. M. Safi, and E. Chung, "Quantitative blood flow estimation in vivo by optical speckle image velocimetry," bioRxiv 2021.03.25.437094 (2021).
32. H. Cheng, Q. Luo, S. Zeng, S. Chen, J. Cen, and H. Gong, "Modified laser speckle imaging method with improved spatial resolution," J. Biomed. Opt. **8**, 559–564 (2003).
33. B. E. A. Saleh and M. C. Teich, *Fundamentals of Photonics*, 2nd ed., (Wiley India, New Delhi, India. 2007).
34. K. S. Park, J. G. Shin, M. M. Qureshi, E. Chung, and T. J. Eom, "Deep brain optical coherence tomography angiography in mice: in vivo, noninvasive imaging of hippocampal formation," Sci. Rep. **8**, 11614 (2018).
35. H. J. Jeon, M. M. Qureshi, S. Y. Lee, and E. Chung, "Optofluidic laser speckle image decorrelation analysis for the assessment of red blood cell storage," PLOS ONE **14**, e0224036 (2019).
36. R. Mostany and C. Portera-Cailliau, "A craniotomy surgery procedure for chronic brain imaging," J. Vis. Exp. **12**, 680 (2008).
37. M. M. Qureshi, J. Brake, H.-J. Jeon, H. Ruan, Y. Liu, A. M. Safi, T. J. Eom, C. Yang, and E. Chung, "In vivo study of optical speckle decorrelation time across depths in the mouse brain," Biomed. Opt. Express **8**, 4855–4864 (2017).

38. Y. Zhang, B. Chen, and D. Li, "Propagation of polarized light in the biological tissue: a numerical study by polarized geometric Monte Carlo method," Appl. Opt. **55**, 2681–2691 (2016).

39. V. Periyasamy and M. Pramanik, "Advances in Monte Carlo simulation for light propagation in tissue," IEEE Rev. Biomed. Eng. **10**, 122–135 (2017).